Cell PRESS
Developmental Cell
Article

Ordered Assembly of the ESCRT-III Complex on Endosomes Is Required to Sequester Cargo during MVB Formation

David Teis,[1] Suraj Saksena,[1] and Scott D. Emr[1,*]
[1]Weill Institute for Cell and Molecular Biology, Cornell University, Ithaca, NY 14853, USA
*Correspondence: sde26@cornell.edu
DOI 10.1016/j.devcel.2008.08.013

SUMMARY

The sequential action of the Vps27/HRS complex, ESCRT-I, -II, and -III is required to sort ubiquitinated transmembrane proteins to the lumen of lysosomes via the multivesicular body (MVB) pathway. While Vps27/HRS, ESCRT-I, and -II are recruited to endosomes as preformed complexes, the ESCRT-III subunits Vps20, Snf7, Vps24, and Vps2 only assemble into a complex on endosomes. We have addressed the pathway and the regulation for ESCRT-III assembly. Our findings indicate the ordered assembly of a transient 450 kDa ESCRT-III complex on endosomes. Despite biochemical and structural similarity, each subunit contributes a specific function. Vps20 nucleates transient oligomerization of Snf7, which appears to sequester MVB cargo. Vps24 terminates Snf7 oligomerization by recruiting Vps2, which subsequently engages the AAA-ATPase Vps4 to dissociate ESCRT-III. We propose that the ordered assembly and disassembly of ESCRT-III delineates an MVB sorting domain to sequester cargo and complete the last steps of MVB sorting.

INTRODUCTION

The ESCRT (*e*ndosomal *s*orting *c*omplex *r*equired for *t*ransport) complexes and their associated proteins compose the machinery required for the formation of *m*ulti*v*esicular *b*odies (MVB) and mediate the lysosomal degradation of transmembrane proteins (Katzmann et al., 2002). ESCRTs are critical for cell surface receptor downregulation, budding of HIV, MHC-II antigen presentation, and cytokinesis (Hurley and Emr, 2006; Saksena et al., 2007). Consequently, the ESCRT machinery is involved in diverse developmental processes, and its dysfunction contributes to many diseases ranging from cancer to neurodegeneration (Piper and Katzmann, 2007; Slagsvold et al., 2006).

Genetic analysis in the yeast *Saccharomyces cerevisae* has led to the identification of 17 class E genes, which constitute the core of the ESCRT machinery. The evolutionarily conserved ESCRT machinery consists of five distinct subcomplexes: the Vps27 complex, ESCRT-I, -II, and -III, and the Vps4 complex (Piper and Katzmann, 2007). Together, they form a protein-protein interaction network that coordinates sorting of ubiquitinated transmembrane proteins and inward budding of the limiting membrane on endosomes. This results in the formation of specialized endosomes known as MVBs. Fusion with the lysosome (in yeast called the vacuole) delivers the MVB vesicles into the lumen of the lysosome, where their cargo is degraded by vacuolar proteases and lipases.

The Vps27/HRS complex, ESCRT-I, and -II function early in the MVB sorting pathway. They are sequentially recruited from the cytoplasm to endosomes as preformed complexes with defined stoichiometry and use distinct ubiquitin-interacting modules to recognize and collect ubiquitinated cargo. Their architecture has been characterized in atomic detail (for summaries see Saksena et al., 2007; Williams and Urbe, 2007). ESCRT-III forms a poorly characterized complex that appears to be critical for late steps in MVB sorting, such as membrane invagination and final cargo sorting. It consists of four core subunits, Vps20, Snf7, Vps24, and Vps2 (Babst et al., 2002a). Unlike other ESCRT complexes, ESCRT-III subunits only assemble into a complex upon recruitment to endosomes. ESCRT-III subunits are similar in size (221–241 amino acids) and have a similar domain organization, with an N-terminal basic and a C-terminal acidic region. The crystal structure of C-terminally truncated human Vps24/CHMP3 (9–183 aa) reveals a molecular architecture that is probably adopted by all ESCRT-III subunits (Muziol et al., 2006). The core of hVps24 forms an asymmetric antiparallel four-helix bundle. The first two helixes, helixes α1 and α2, form a 70 Å hairpin, which is required for membrane interaction and homo- or heterodimerization. The C-terminal acidic portion is called the autoinhibitory region and comprises helix α5 and the MIT (microtubule-interacting and transport)-interacting region (MIR) (Obita et al., 2007; Scott et al., 2005a, 2005b; Stuchell-Brereton et al., 2007). It undergoes competing interactions with helix α2 of the core and thus prevents premature hetero- and homodimerization. Autoinhibition of ESCRT-III subunits generates metastable ''closed'' ESCRT-III monomers in the cytoplasm, and its release appears required for ESCRT-III assembly (Muziol et al., 2006; Shim et al., 2007; Zamborlini et al., 2006). Genetic and biochemical analyses place ESCRT-II directly upstream of ESCRT-III and therefore suggest a role for ESCRT-II in initiating the formation of the ESCRT-III complex on endosomes (Babst et al., 2002b; Teo et al., 2004).

The stoichiometry and the size of the ESCRT-III complex on the endosome are not known. Our previous studies have suggested that ESCRT-III consists of two distinct subcomplexes, the Vps20-Snf7 and the Vps2-Vps24 subcomplexes (Babst et al., 2002a). The Vps20-Snf7 subcomplex binds to the endosomal membrane, in part through the N-terminal myristoylation of Vps20. Additionally, Vps20 binds directly to Vps25 of ESCRT-II (Teo et al., 2004). The Vps2-Vps24 subcomplex binds to the

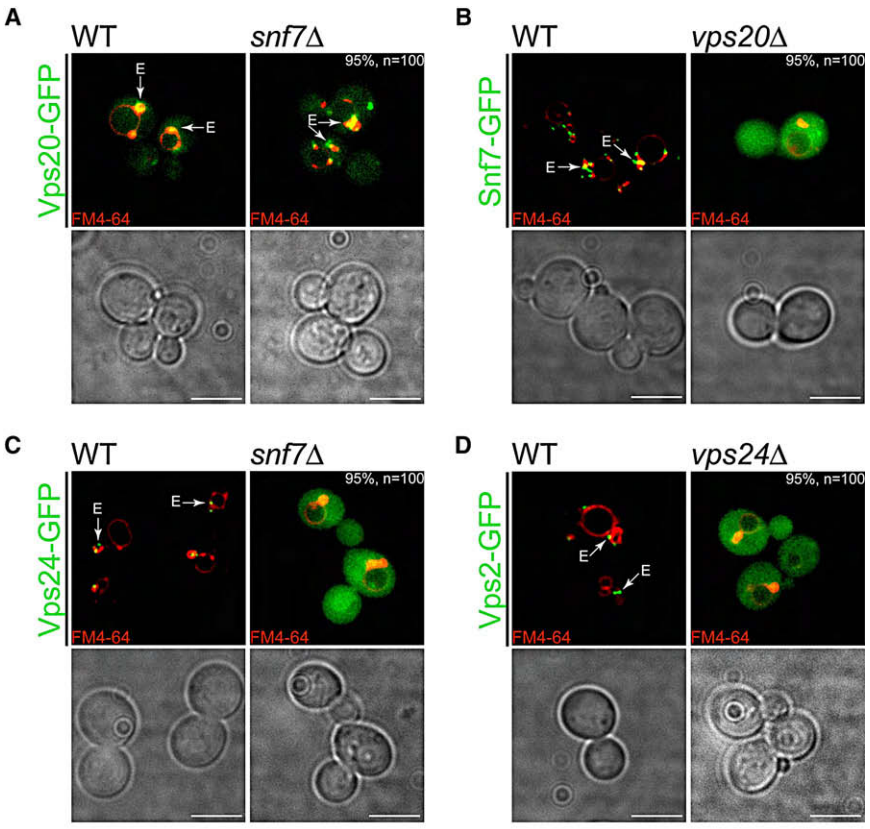

E

	Endosomes	Cytoplasm
Vps20-GFP	*snf7Δ, vps24Δ*	-
Snf7-GFP	*vps24Δ, vps2Δ*	*vps20Δ*
Vps24-GFP	*vps2Δ*	*snf7Δ*
Vps2-GFP	-	*snf7Δ, vps24Δ*

F

Vps20
↓
Snf7
↓
Vps24
↓
Vps2

Figure 1. ESCRT-III Assembles in a Sequential Manner on Endosomes

Live cell microscopy of cells harboring chromosomal integrations for *VPS20*-GFP, *SNF7*-GFP, *VPS24*-GFP, and *VPS2*-GFP. GFP is shown in green. FM4-64 is shown in red. Size bar = 5 μm.

(A) Vps20-GFP localized to cytoplasm and to endosomes (arrow) the in *snf7Δ* mutants.

(B) Snf7-GFP localized to endosomes (arrow) and mislocalized to the cytoplasm in *vps20Δ* mutants.

(C) Vps24-GFP localized to endosomes (arrow) and mislocalized to the cytoplasm in *snf7Δ* mutants.

(D) Vps2-GFP localized to endosomes (arrow) and mislocalized to the cytoplasm in *vps24Δ* mutants.

(E) Localization of ESCRT-III-GFP in different ESCRT-III mutants.

(F) Order of assembly of ESCRT-III on endosomes.

Vps20-Snf7 subcomplex and recruits the AAA-ATPase, Vps4, to endosomes (Babst et al., 2002a). In particular, the direct interaction of the MIT-interacting motif (MIM) of Vps2 with the MIT domain at the N terminus of Vps4 is required for MVB sorting (Obita et al., 2007; Stuchell-Brereton et al., 2007). Yeast two-hybrid and biochemical studies indicate a complex network of homo- and heteromeric interactions among ESCRT-III subunits (Bowers et al., 2004; von Schwedler et al., 2003). When ESCRT-III subunits are present at a high concentration, either in vivo upon overexpression or in vitro, they can oligomerize and even form filaments at the plasma membrane (PM) that inhibit viral budding and endosomal function (Lin et al., 2005; Zamborlini et al., 2006). Yet, how the four core subunits interact to form a functional ESCRT-III complex on endosomes, that contributes the final steps of MVB sorting, is not understood.

Here we show that the assembly of the ESCRT-III complex occurs in a sequential, well-ordered manner on the surface of endosomes. Vps20 is essential to nucleate the transient oligomerization of Snf7 at the endosome. The Snf7 oligomer contributes the major building unit of a transient 450 kDa ESCRT-III complex. In vivo quantification experiments suggest that at least 50% of ESCRT-III consist of Snf7 oligomers. The Vps24-Vps2 subcomplex caps and terminates the transient Snf7 oligomer by recruiting Vps4, which then dissociates ESCRT-III. In addition, we provide evidence that Snf7 oligomers sequester cargo at the endosome. Our findings suggest that regulated Snf7 oligomerization is required to delineate an MVB-sorting domain and thereby commits cargo to complete the last step of MVB sorting.

RESULTS

ESCRT-III Assembles in a Sequential Manner on Endosomes

Genetic analysis in yeast has led to the identification of four core ESCRT-III subunits, Vps20, Snf7, Vps24, and Vps2 (Babst et al., 2002a). To begin to understand the molecular architecture of ESCRT-III, we first determined the order of ESCRT-III assembly at the endosomes. C-terminal GFP fusions of all four ESCRT-III core subunits were generated by chromosomal integration. In wild-type cells, the ESCRT-III-GFP fusions exhibited a dominant-negative phenotype. The bulky GFP tag interfered with autoinhibition, as reported for the mammalian homologs (Martin-Serrano et al., 2003; Strack et al., 2003) (Zamborlini et al., 2006). ESCRT-III-GFP subunits caused a block of MVB sorting and accumulated on enlarged endosomes (class E compartments) (Figure 1). Consequently, mutants that interfere directly with membrane recruitment of ESCRT-III-GFP subunits can be easily identified. This has allowed us to establish the order of assembly for the ESCRT-III subunits.

Vps20-GFP localized to the cytoplasm and to endosomes, independently of other ESCRT-III subunits (Figures 1A and 1E). Snf7-GFP was mislocalized from endosomes into the cytoplasm in *vps20Δ* mutants (Figure 1B). In contrast, loss of *VPS24*, *VPS2*, or *VPS4* did not affect the localization of Snf7-GFP (Figure 1E; data not shown). Recruitment of Vps24-GFP to endosomes

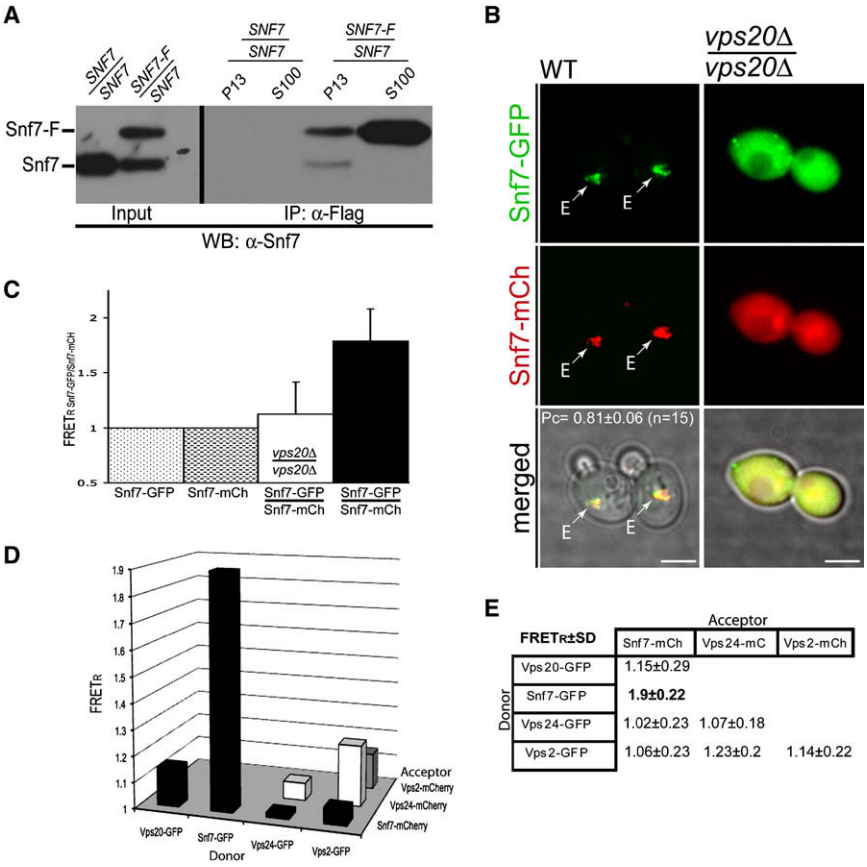

Figure 2. Vps20 Is Required to Induce Oligomerization of Snf7 on Endosomes

(A) Diploid cells harboring one *SNF7* and one *SNF7-Flag* allele were fractionated and solubilized. The solubilized fractions were subjected to immunoprecipitations (IPs). Inputs (10%) and IPs were separated by SDS-PAGE and analyzed with the indicated antibody. Snf7-Flag specifically co-IPs Snf7 from membranes (lane 4) but not from the cytoplasm.

(B) Representative images of diploid cells carrying one *SNF7*-GFP and *SNF7*-mCherry allele in WT cells and in *vps20Δ/vps20Δ* mutants. Arrows indicate colocalization of Snf7-GFP and Snf7-mCherry. Pixel-by-pixel colocalization analysis yielded a Pearson coefficient (P_c) of correlation with Snf7-mCherry, $P_{cSnf7\text{-}GFP}$ = 0.81 ± 0.06 (n = 15). Size bar = 5 μm.

(C) Pixel-by-pixel fluorescence resonance energy transfer (FRET) analysis based on the FRET ratio. $FRET_R$ = 1.78 ± 0.29 (n = 27). In *vps20Δ/vps20Δ* mutants the $FRET_R$ dropped to $FRET_R$ = 1.12 ± 0.29 (n = 29). $FRET_R$ = 1 is no FRET. Error bars represent SD.

(D and E) (D) $FRET_R$ of ESCRT-III. The corresponding donors/acceptor pairs are indicated. $FRET_R$ values are listed in the table (E).

required Snf7 (Figure 1C), but not Vps2 (Figure 1E). Recruitment of Vps2-GFP to endosomes required Vps24 as well as Snf7 (Figures 1D and 1E). These findings show that ESCRT-III is assembled in a sequential manner (Figure 1F). Vps20-dependent recruitment of Snf7 may be the first step in the membrane-dependent formation of ESCRT-III (Figure 1F).

Vps20 Is Required to Induce Oligomerization of Snf7 on Endosomes

Vps20 is the only ESCRT-III subunit required to recruit Snf7-GFP to endosomes (Figure 1). Snf7 exists as a soluble "closed" monomer in the cytoplasm and is not recruited as a preformed complex (see Figures S1A–S1C available online). To investigate how Vps20 recruits Snf7 to endosomes, we tested whether Vps20 is required to induce oligomerization of Snf7 on endosomes.

First, we addressed whether the ESCRT-III complex on endosomes contains multiple copies of Snf7 by using immunoprecipitation. For this purpose, a diploid strain carrying one *SNF7* wild-type allele and a second *SNF7*-Flag allele was generated (Figure 2A). The resulting diploid strain exhibited normal sorting via the MVB pathway (data not shown). Following separation of membrane and cytoplasm fractions, Snf7-Flag was immunoprecipitated. Snf7 coimmunoprecipitated specifically with Snf7-Flag from endosomes and not from the cytoplasm (Figure 2A). Vps24-Flag coimmunoprecipitated Snf7 efficiently but did not coimmunoprecipitate itself (Figure S1F). These findings showed that multiple Snf7, but not multiple Vps24, molecules are present in the ESCRT-III complex, suggesting that Vps20 induces oligomerization of Snf7.

hSnf7 is capable of forming filaments at the plasma membrane when overexpressed (Hanson et al., 2008), and hVps24 crystallizes in a linear lattice (Muziol et al., 2006). Given the high sequence similarity among ESCRT-III subunits, we reasoned that Snf7 may assemble in a homo-oligomer on endosomes that could be analyzed using fluorescence resonance energy transfer (FRET) in vivo. If Snf7 forms a homo-oligomer, GFP fused to the C terminus of one Snf7 molecule and mCherry fused to the C terminus of another Snf7 molecule should be sufficiently close together (≤88 Å) to allow FRET. However, if Snf7 molecules are not side-by-side and preferentially interact with other ESCRT-III subunits, FRET between Snf7-GFP and Snf7-mCherry would be blocked. Thus, efficient Snf7-Snf7 FRET would indicate Snf7 oligomerization on endosomes in vivo.

To test Snf7-Snf7 FRET, we generated a diploid yeast strain carrying one chromosomal allele of *SNF7*-GFP and a second chromosomal allele of *SNF7*-mCherry. Snf7-GFP colocalized with Snf7-mCherry on endosomes. Pixel-by-pixel colocalization analysis was performed using the Pearson coefficient of correlation (P_c). A P_c = 1 indicates perfect colocalization. Snf7-GFP and Snf7-mCherry had a P_c = 0.81 ± 0.06 (n = 15), suggesting significant colocalization (Figure 2B). In a diploid *SNF7-GFP/SNF7-mCherry* strain that lacked both alleles of *VPS20*, Snf7-GFP and Snf7-mCherry mislocalized into the cytoplasm (Figure 2B).

To measure FRET between Snf7-GFP and Snf7-mCherry on endosomes in vivo, we utilized a simple and robust method based on FRET ratio ($FRET_R$) (Muller et al., 2005). $FRET_R$ calculations revealed efficient FRET between Snf7-GFP and Snf7-mCherry on endosomes. Snf7-GFP and Snf7-mCherry on

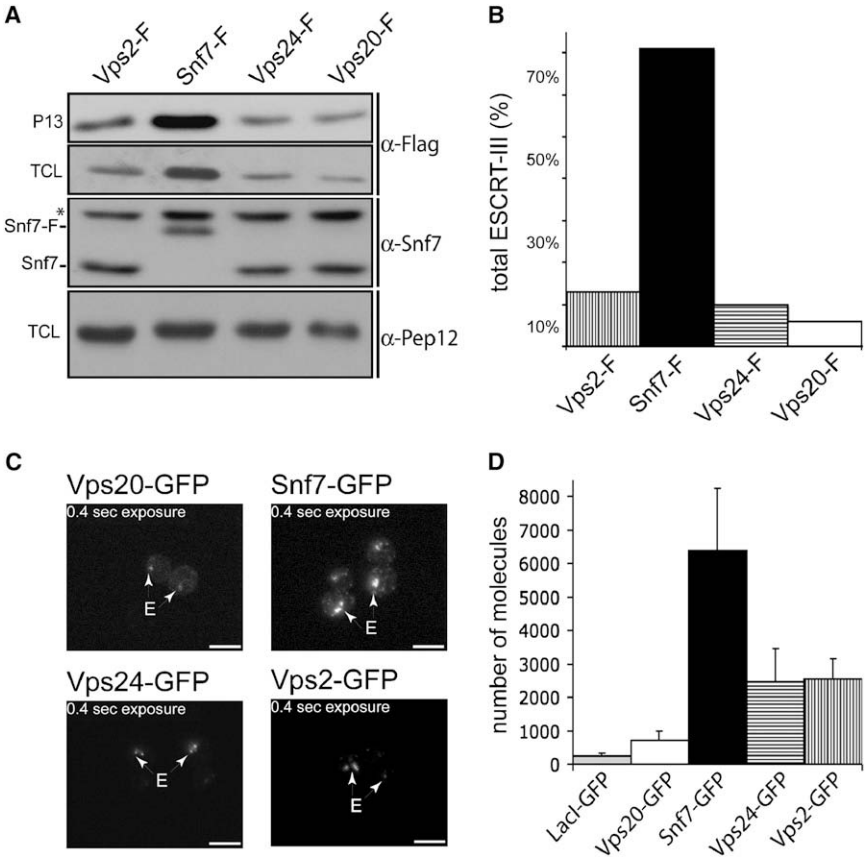

Figure 3. Snf7 Is the Most Abundant ESCRT-III Subunit

(A) A 3×Flag tag was integrated at the C terminus of *VPS2*, *SNF7*, *VPS24*, and *VPS20*. Membrane fractions (P13) or total cell lysates (TCL) were analyzed by SDS-PAGE and western blot. *Background band.

(B) Densitometric analysis of anti-Flag western blot from membrane fractions (P13).

(C) Representative images of Vps2-GFP, Snf7-GFP, Vps24-GFP, and Vps20-GFP at 0.4 s exposure. Size bar = 5 μm. Arrows point to endosomes.

(D) Total fluorescence intensity (I_F) of cells was measured and background subtracted. To obtain the number of molecules, I_F was normalized against I_F of the 256 LacI-GFP molecules. Error bars represent SD.

endosomes have a $FRET_R$ of 1.78 ± 0.29 (n = 27) (Figures 2B and 2C). In the *vps20Δ/vps20Δ* mutant, Snf7-GFP and Snf7-mCherry redistribute to the cytoplasm and the $FRET_R$ dropped to 1.12 ± 0.29 (n = 29), which is very close to no FRET ($FRET_R$ = 1) (Figures 2B and 2C). The ratio of fluorescence intensity (I_F) remained relatively constant: 0.88 ± 0.2 (n = 15) and 0.76 ± 0.1 in the *vps20Δ/vps20Δ* strain (n = 15) (Figure S1D). To address whether Snf7-Snf7 FRET is the result of homo-oligomerization or of an alternative oligomeric ESCRT-III arrangement, we next tested all other possible hetero and homo-FRET combinations (n ≥ 49 for all FRET pairs) (Figures 2D and 2E). Significant FRET ($FRET_R$ = 1.9 ± 0.22) was measured for Snf7-Snf7, whereas other homo-FRET combinations with Vps24-Vps24, or Vps2-Vps2 showed low $FRET_R$ (Figures 2D and 2E and Figure S3). Snf7-mCherry and other ESCRT-III-GFP subunits only partially colocalize and show low $FRET_R$ (Figures 2D, 2E, and 4C). These results suggest that Snf7-Snf7 FRET is most likely a consequence of a homo-oligomeric arrangement of Snf7 on endosomes.

Taken together, the results from the coimmunoprecipitation and FRET experiments suggest that Vps20 nucleates Snf7 homo-oligomerization on endosomes.

Snf7 Is the Most Abundant ESCRT-III Subunit

We next determined the relative abundance of each core ESCRT-III subunit. A C-terminal 3×Flag tag was integrated into the genomic locus of each ESCRT-III gene. C-terminal 3×Flag tagging did not interfere with the function of ESCRT-III subunits (data not shown) and did not affect protein expression levels, as demonstrated for Snf7-Flag, using the native Snf7 antibody (Figure 3A, panel 3). Importantly, densitometric analysis of western blots from total cell lysates (TCL) or from membrane fractions (P13) revealed that Snf7-Flag was the most abundant of the ESCRT-III subunits and approximately ten times more abundant in TCL and on membranes fraction as compared to Vps20-Flag (Figures 3A and 3B).

Next, we measured the approximate number of molecules per cell for each individual ESCRT-III subunit. For this purpose, we first measured the fluorescence intensity (I_F) of a known standard. We used a reporter yeast strain that harbors an array of 128 LacO operators integrated in the INO3 gene and LacI-GFP integrated at the HIS3 locus (Brickner and Walter, 2004). Two LacI molecules bind one LacO operator; thus, the LacI-GFP I_F corresponds to 256 molecules. Quantitative image analysis was used to determine the I_F of 256 LacI-GFP molecules per cell (Supplemental Data and Figure S2). We next recorded fluorescence images of all four ESCRT-III-GFP subunits using identical microscope and camera settings (Figure 3C). Fluorescence quantification revealed that Snf7 was the most abundant ESCRT-III subunit (Figure 3D), which is consistent with the result obtained by western blot analysis (Figures 3A and 3B). In addition, for each ESCRT-III subunit, we were able to measure the approximate number of molecules/cell: Vps20 = 700 ± 250 (consistent with SGD: 950), Snf7 = 6400 ± 1840 (SGD: 3270), Vps24 = 2500 ± 960 (SGD: 1890), and Vps2 = 2500 ± 600 (SGD: not visualized). Quantification of the four ESCRT-III core subunits by semiquantitative western blot analysis and quantitative image analysis demonstrates that Snf7 is the most abundant ESCRT-III subunit. This finding supports the idea that Vps20 nucleates oligomerization of Snf7. Moreover, these data suggest that ESCRT-III is not likely to be a 1:1:1:1 complex, an important insight in deciphering the molecular architecture of ESCRT-III.

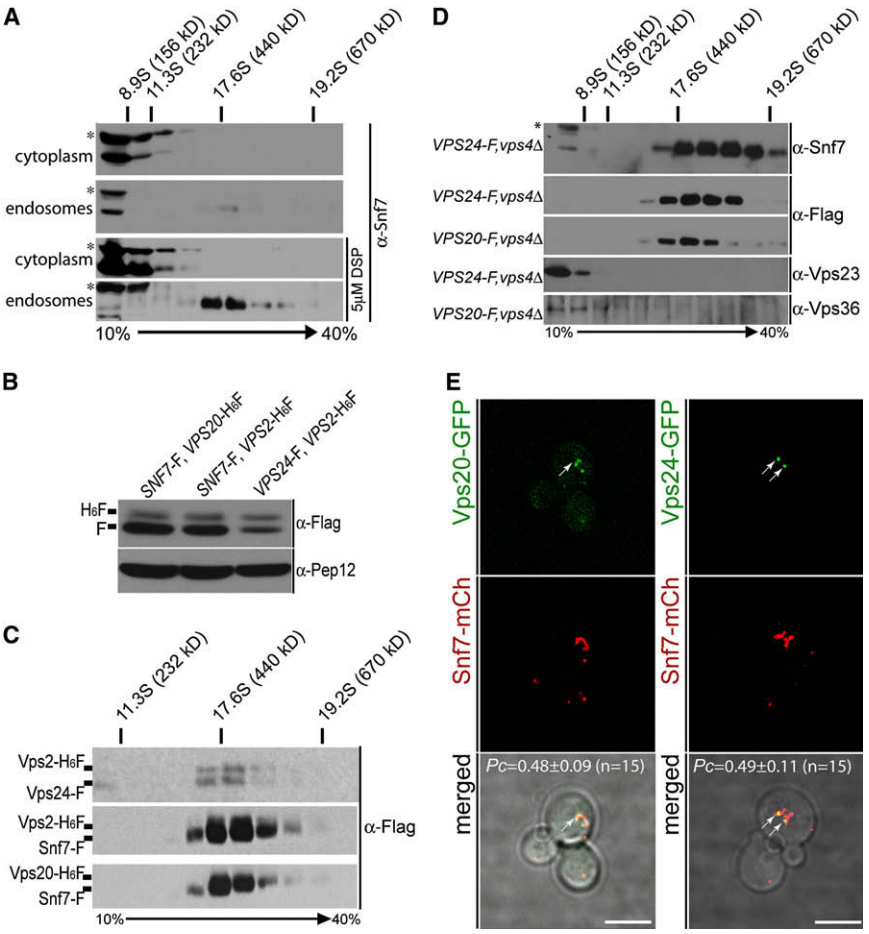

Figure 4. ESCRT-III Assembles into a Transient 450 kDa Complex on Endosomes

(A) Spheroplasts were either left untreated or crosslinked with 5 μm DSP for 15 min and fractionated. Membrane fractions (P13) and cytoplasm (S100) were solubilized and subjected to velocity sedimentation and analyzed by SDS-PAGE and western blot. *Background band.

(B) Membrane fractions of *SNF7-Flag, VPS20-H6-Flag* and *SNF7-Flag, VPS2-H_6-Flag* and *VPS24-Flag, VPS2-H_6-Flag* were analyzed by SDS-PAGE and western blot.

(C) Spheroplasts of *SNF7-Flag, VPS20-H_6-Flag* and *SNF7-Flag, VPS2-H_6-Flag* and *VPS24-Flag, VPS2-H_6-Flag* were crosslinked with 5 μm DSP. Solubilized membrane fractions (P13) were subjected to velocity sedimentation and analyzed by SDS-PAGE and western blot.

(D) Solublized membrane fractions of *VPS24-Flag*, *vps4Δ*, or *VPS20-Flag, vps4Δ* were subjected to velocity sedimentation and analyzed by SDS-PAGE and western blot with the indicated antibodies. *Background band.

(E) Representative images of cells harboring *VPS20*-GFP and *SNF7*-mCherry or *VPS24*-GFP and *SNF7*-mCherry. Pixel-by-pixel colocalization analysis yielded a Pearson coefficient (P_c) of correlation with Snf7-mCherry. $P_{cVps20\text{-}GFP}$ = 0.49 ± 0.11 (n = 15), $P_{cVps24\text{-}GFP}$ = 0.48 ± 0.09 (n = 15). P_c = 1 represents perfect colocalization. Size bar = 5 μm.

ESCRT-III Forms a Transient 450 kDa Complex on Endosomes

Size-exclusion chromatography from yeast cytoplasm or with purified recombinant H_6-Snf7 from *E. coli* (Figures S1A and S1B) together with coimmunoprecipitation and FRET experiments (Figure 2) indicated that soluble Snf7 is most likely monomeric in solution. Using velocity sedimentation centrifugation on 10%–40% glycerol gradients, we attempted to determine the sedimentation of Snf7 from solubilized membranes (P13) or cytosol (S100). Cytosolic Snf7 as well as purified recombinant H_6-Snf7 from *E. coli* sedimented in a low molecular weight fraction (M_r < 156 kDa) (Figure 4A and Figure S1C). Analysis of Snf7 from solubilized membranes showed that the majority of Snf7 sediments in a low molecular weight fraction (M_r < 156 kDa). However, a small fraction of Snf7 was detected at about 450 kDa, suggesting a transient higher molecular weight complex containing Snf7 (Figure 4A).

ESCRT-III subunits cycle between cytoplasmic monomers and the assembled complex on endosomes. Therefore, we next tested whether in vivo crosslinking would stabilize an ESCRT-III complex on endosomes. Cells were spheroplasted, incubated for 15 min with 5 μM DSP (a short, 12 Å long, cleavable and membrane-permeable crosslinker), and fractionated into cytosol and membrane. The solubilized fractions were subjected to velocity sedimentation centrifugation. Cytoplasmic Snf7 did not crosslink. However, endosomal Snf7 was crosslinked into a stable complex of about 450 kDa (Figure 4A). These results support the hypothesis that the cytoplasmic pool exists in a closed nonreactive conformation and that recruitment to endosomes activates ESCRT-III subunits to form a transient 450 kDa ESCRT-III complex.

To address the relative abundance of ESCRT-III subunits in the crosslinked complex, cells were generated that carry a C-terminal 3×Flag tag integrated into the genomic locus of one ESCRT-III subunit and a C-terminal 6×His-3×Flag tag integrated into the genomic locus of a second ESCRT-III subunit (Figure 4B). These strains exhibited normal protein sorting via the MVB pathway (data not shown) and allowed the simultaneous detection of two ESCRT-III subunits with the same antibody. Cells were spheroplasted and crosslinked as before, and solubilized membrane fractions were subjected to velocity sedimentation centrifugation. The signal of the Snf7 band was so intense that it masked the very weak Vps2 and Vps20 bands. These experiments demonstrated that Snf7 is the most abundant subunit in the 450 kDa ESCRT-III complex (Figure 4C), whereas Vps24 and Vps2 are present at equimolar ratios and the nucleator Vps20 is the least abundant (Figure 4C).

The AAA-ATPase Vps4 provides the catalytic activity for the dissociation of ESCRT-III. Inactivation of Vps4 should therefore accumulate ESCRT-III on endosomes. Solubilized membrane

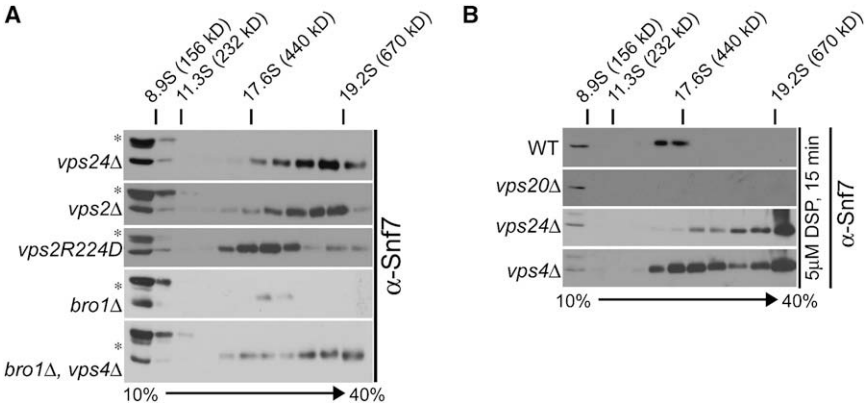

Figure 5. The Vps24/Vps2 Subcomplex Terminates Snf7 Oligomerization by Recruiting Vps4

(A) Solubilized membrane fractions (P13) of *vps24Δ*, *vps2Δ*, *vps2R224D*, *bro1Δ*, or *bro1Δ, vps4Δ* cells were subjected to velocity sedimentation and analyzed by SDS-PAGE and western blot. (B) Spheroplasts of WT, *vps20Δ*, *vps24Δ*, and *vps4Δ* were crosslinked with 5 μm DSP for 15 min and fractionated. Membrane fractions (P13) were solubilized and subjected to velocity sedimentation and analyzed by SDS-PAGE and western blot. *Background band.

fractions from *vps4Δ* mutant cells were subjected to velocity sedimentation centrifugation. Blocking ESCRT-III dissociation generated a high molecular weight ESCRT-III complex (>450 kDa) and resulted in cosedimentation of Vps20, Vps24, and Snf7 (Figure 4D). Together with coimmunoprecipitation experiments from the membrane fractions (Figure S1E) and the crosslinking experiments, we conclude that all ESCRT-III subunits are represented in the same complex (Figure 4D), yet a very different ratios. Surprisingly, subunits of ESCRT-I (Vps23) and ESCRT-II (Vps36) did not cosediment and are detected at a lower molecular weight, consistent with their monomeric complex molecular weights (M_r < 156 kDa) (Figure 4C). Our fractionation and solubilization procedure may disrupt the interactions of ESCRT-I and ESCRT-II with the ESCRT-III complex, whereas the ESCRT-III oligomer is stable. It is therefore tempting to speculated that a 450 kDa ESCRT-III complex would comprise approximately 17 ESCRT-III subunits, each having an M_r of 27 kDa. According to the quantification, 10–15 Snf7 molecules could form an oligomer in each 450 kDa complex.

To further investigate how ESCRT-III assembles at the endosome, we used fluorescence microscopy and image analysis to determine the colocalization of different ESCRT-III subunits. Vps20-GFP as well as Vps24-GFP only partially colocalized with Snf7-mCherry at the endosomes (Figure 4E). Vps20-GFP was found in the cytoplasm and on endosomes, whereas Vps24-GFP was often localized in two punctae on endosomes (50% of all E compartments, Figure S2C), which decorated larger Snf7-mCherry structures (Figure 4E), possibly similar to filaments formed by hSnf7 at the plasma membrane (Hanson et al., 2008). To measure the colocalization between the different ESCRT-III molecules, pixel-by-pixel analysis was employed and the Pearson coefficient of correlation (P_c) with Snf7-mCherry was calculated. This analysis revealed partial colocalization of Vps20-GFP with Snf7-mCherry ($P_{cVps20\text{-}GFP}$ = 0.49 ± 0.11; n = 15) and partial colocalization of Vps24-GFP with Snf7-mCherry ($P_{cVps24\text{-}GFP}$ = 0.48 ± 0.09; n = 15) (Figure 4C and Figure S2B). Thus, the formation of distinct patches of Snf7 and Vps24 or Vps20 suggests that they are not intermixed, which is confirmed by low FRET among other ESCRT-III subunits (Figures 2D and 2E). In contrast, Snf7-GFP showed significant colocalization with Snf7-mCherry ($P_{cSnf7\text{-}GFP}$ = 0.81 ± 0.06) and they form a good FRET-pair (Figure 2). These results are most consistent with a Snf7 homo-oligomer.

The Vps24-Vps2 Subcomplex Terminates Snf7 Oligomerization by Recruiting Vps4

Thus far our results indicate that Vps20-induced Snf7 oligomerization is the first step in the formation of ESCRT-III at the endosome. Therefore, we next addressed how Vps24 and Vps2 contribute to the formation of the ESCRT-III lattice. We have previously shown that the Vps24-Vps2 subcomplex is required to efficiently recruit Vps4 to endosomes (Babst et al., 2002a; Nickerson et al., 2006). Deletion of *VPS24* or *VPS2* resulted in the accumulation of ESCRT-III as a high molecular weight (>500 kDa) complex on endosomes as determined by velocity sedimentation centrifugation (Figure 5A). Importantly, in *vps24Δ* mutant cells, Vps2 as well as Vps4 are no longer recruited to endosomes. Moreover, Snf7 is ten times more abundant than Vps20. Therefore, this finding suggested that ESCRT-III consists mainly of Snf7 oligomers.

Alternatively, a binding partner of Snf7, Bro1 (Luhtala and Odorizzi, 2004; Odorizzi et al., 2003), could significantly contribute to the high molecular weight of ESCRT-III. However deletion of *bro1* alone does not affect ESCRT-III assembly (Figure 5A). Moreover in *bro1Δ*, *vps4Δ* mutants, ESCRT-III still assembled into a high molecular weight complex, demonstrating that Bro1 does not significantly contribute to the formation of ESCRT-III (Figure 5A). Therefore, it is more likely that Bro1 uses Snf7 oligomers as a docking platform to recruit Doa4, allowing deubiquitination of cargo at Snf7 oligomers.

Two recent studies defined an MIM (MIT-interacting motif) in Vps2, which is required for the direct interaction with the MIT (microtubule interacting and transport) domain of Vps4 (Obita et al., 2007; Stuchell-Brereton et al., 2007). To test if the interaction of Vps4 with the MIM domain of Vps2 is required to dissociate ESCRT-III, we used the *vps2R224D* point mutant. The R224D mutation in the MIM domain of Vps2 abolished binding to the MIT domain of Vps4 in vitro (Obita et al., 2007). In *vps2R224D* mutant cells, ESCRT-III accumulated as a 450 kDa complex, which is smaller as compared with *vps24Δ* or *vps2Δ* mutant cells (Figure 5A). It seems likely that in the *vps2R224D* mutant cells, the Vps4-dependent dissociation of ESCRT-III is not completely blocked, but slowed down. This finding is consistent with the partial CPS sorting defect in the *vps2R224D* mutant cells (Obita et al., 2007), whereas deletion of *VPS2* or *VPS24* results in a block in CPS sorting. Together these findings indicate that Vps24 terminates the formation of Snf7 oligomers by recruiting Vps2,

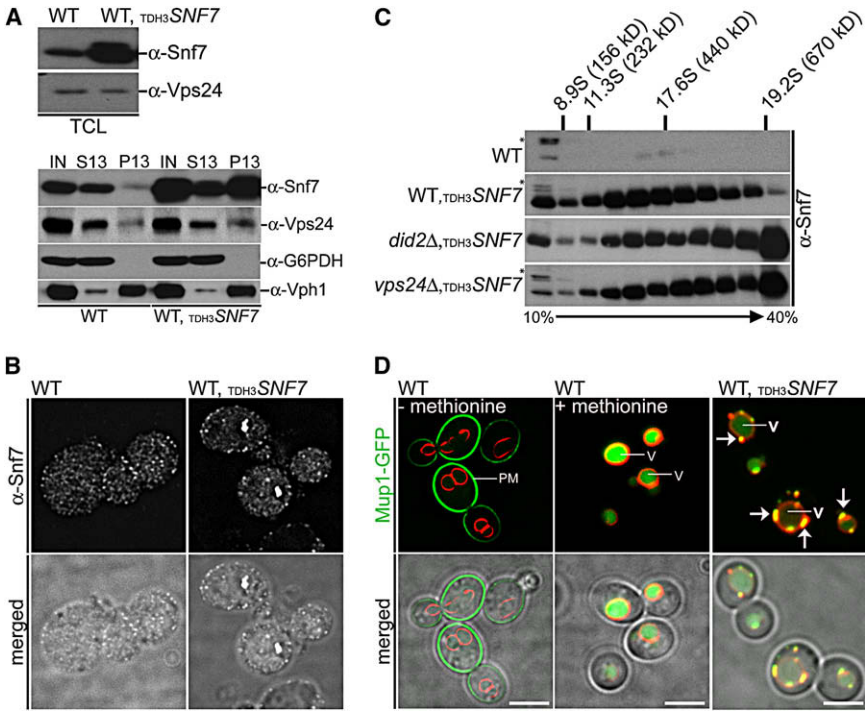

Figure 6. Excess of Snf7 Alters ESCRT-III Assembly

(A) Total cell lysate and subcellular fractions (S13 and P13) of WT cells and WT,$_{TDH3}$*SNF7* were analyzed by SDS-PAGE and western blot.

(B) Indirect immunofluorescence using the anti-Snf7 antibody of WT cells and WT,$_{TDH3}$*SNF7*.

(C) Spheroplasts of WT; WT,$_{TDH3}$*SNF7*; *did2Δ*, $_{TDH3}$*SNF7*; *vps24Δ*, $_{TDH3}$*SNF7* were fractionated. Membrane fractions (P13) were solubilized and subjected to velocity sedimentation and analyzed by SDS-PAGE and western blot. *Background band.

(D) Representative images of WT and WT,$_{TDH3}$*SNF7* cells expressing Mup1-GFP (green). Cells were treated for 60 min with methionine and FM4-64 (red). Arrows indicate large perivacuolar vesicle-like structures. Vacuole (V), plasma membrane (PM).

which initiates ESCRT-III dissociation via its MIM domain interaction with the MIT domain of Vps4.

To test a possible terminator/capping function for Vps24, we performed in vivo crosslinking experiments in different ESCRT-III mutants. Cells were spheroplasted, incubated for 15 min with 5 μM DSP, and fractionated into cytosol and membrane. The solubilized membrane fractions were subject to velocity sedimentation centrifugation. In wild-type cells, Snf7 was crosslinked into a 450 kDa complex (Figure 5B). In *vps20Δ* mutant cells Snf7 did not crosslink. Thus, deletion of the nucleator Vps20 resulted in loss of Snf7 oligomerization. If Vps24 terminates Snf7 oligomerization, Snf7 should crosslink into a high molecular weight oligomer in *vps24Δ* mutant cells. In *vps24Δ* mutant cells, Snf7 crosslinked in a complex that sedimented to the bottom of the gradient (>670 kDa) (Figure 5B). In a *vps24Δ* mutant cell, ESCRT-III contains mainly Vps20 and Snf7. Since Snf7 is ten times more abundant than Vps20, ESCRT-III in a *vps24Δ* mutant consists mostly of Snf7 oligomers. In *vps4Δ* mutant cells, Snf7 accumulated as a 450 kDa complex and at the bottom of the gradient, suggesting that Snf7 oligomerization was terminated (at 450 kDa), until Vps24 was depleted (>670 kDa) (Figure 5B). These findings show that Vps20 is required for Snf7 oligomerization and that the Vps24-Vps2 subcomplex terminates this process by recruiting Vps4 for ESCRT-III dissociation. Using the same assay, we investigated the role of the ESCRT-III-associated proteins Did2 and Vps60. Deletion of *DID2* or *VPS60* did not significantly affect ESCRT-III assembly or disassembly as indicated by the formation of a 450 kDa ESCRT-III complex. (Figure S4A). However, in a *did2Δ*, *vps60Δ* double mutant, Snf7 shifted into a high molecular weight complex (Figure S4A). These findings are consistent with a nonessential role for Did2 and Vps60 as ESCRT-III-associated proteins that coordinate Vps4 activity (Azmi et al., 2008; Dimaano et al., 2008; Nickerson et al., 2006; Rue et al., 2008).

Based on these results, we propose a model for the ordered assembly and the molecular architecture of ESCRT-III. Vps20 nucleates Snf7 oligomerization into a membrane-associated filament, which is terminated by the Vps24-Vps2 subcomplex through the recruitment of Vps4, which subsequently dissociates ESCRT-III.

Excess Snf7 Alters ESCRT-III Assembly

To test how the size of the ESCRT-III oligomer is regulated, we decided to induce stoichiometric imbalance by overexpressing Snf7 from the TDH3-promotor (SGD: 169,000 molecules/cell). Subcellular fractionation experiments demonstrated that Snf7 is mainly cytoplasmic; however, when Snf7 was overexpressed (>20-fold), it accumulated on membranes and not in the cytoplasm (Figure 6A). Importantly, the protein levels and the distribution of Vps24 did not change. Indirect immunofluorescence microscopy using the Snf7 antibody (Babst et al., 1998) confirmed that Snf7 is mostly cytoplasmic and upon overexpression accumulated on subcellular structures, most likely endosomes (Figure 6B). Moreover, velocity sedimentation analysis of solubilized membrane fractions demonstrated that overexpressed Snf7 accumulated in high molecular weight complexes (Figure 6C). These findings would be most consistent with insufficient capping capacity, which would favor Snf7 oligomerization. To test this idea, we overexpressed Snf7 in a *did2Δ* mutant, because Did2 is not essential for ESCRT-III function but modulates the function of Vps4-dependent ESCRT-III disassembly. When Snf7 is overexpressed in *did2Δ* mutant cells, Snf7 assembles into a very high molecular weight complex mimicking loss of Vps24 (Figure 6C). Taken together, these results imply that Snf7 can form homo-oligomeres on endosomes. Under normal conditions, Snf7 oligomerization is capped by Vps24. Upon excess Snf7, Vps24-dependent capping activity becomes limiting and leads to enhanced Snf7 homo-oligomerization. Thus, the relative stoichiometry of ESCRT-III subunits is an important factor in ESCRT-III assembly and dissociation.

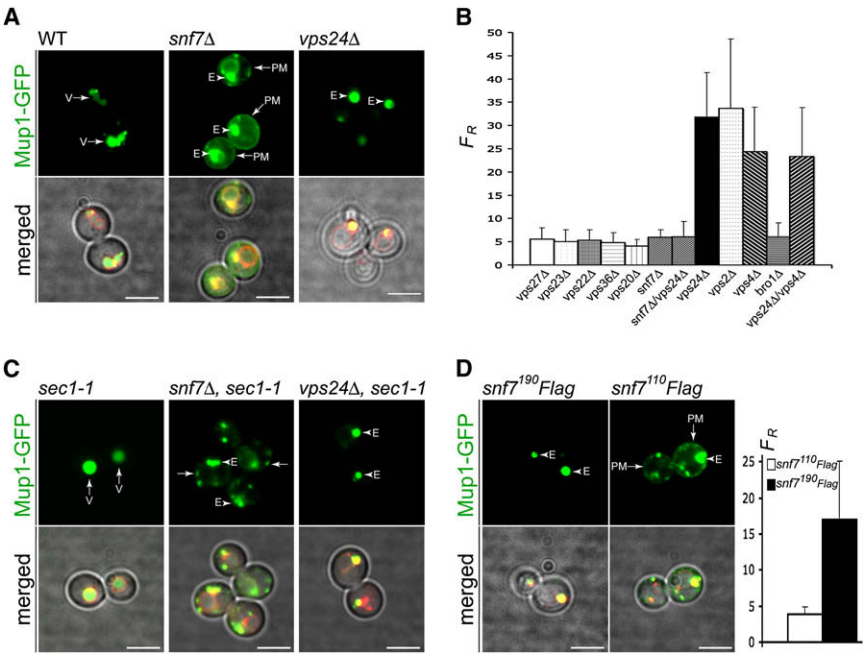

Figure 7. Snf7 Oligomerization Is Required to Trap MVB-Cargo

(A) Representative images of cells expressing Mup1-GFP (green). Cells were treated for 60 min with methionine and FM4-64 (red). In *snf7Δ* cells, Mup1-GFP accumulates on the E compartment (arrowheads) and is detected at the PM (arrows). In *vps24Δ*, Mup1-GFP is detected only on the E compartment.

(B) Fluorescence ratio (F_R) of Mup1-GFP at the PM and on the endosomes in different class E mutants. Trapping cargo at the E compartment requires Snf7 oligomerization. n > 25 for each mutant.

(C) Representative images of cells expressing Mup1-GFP (green). Cells were treated for 60 min with methionine and subsequently shifted to non-restrictive temperature for 60 min. In *snf7Δ, sec1-1* cells, Mup1-GFP accumulates on the E compartment (arrowheads) and also in new vesicular structures (arrows). In *vps24Δ, sec1-1*, Mup1-GFP is detected only on the E compartment.

(D) Representative images of *snf7* mutant cells expressing Mup1-GFP (green). Cells were treated for 60 min with methionine. $snf7^{110}$*Flag* permits Mup1-GFP recycling. $snf7^{190}$*Flag* traps MUP1-GFP at the E compartment (arrowheads). Fluorescence ratio (F_R) of Mup1-GFP fluorescence in the two different *snf7* mutants (n = 30). Error bars represent SD.

The Snf7 Oligomer Is Required to Sequester MVB Cargo

While it is clear that ESCRT-III is required for a late step in the MVB sorting process, it is not understood how ESCRT-III contributes to the sorting reaction. Because oligomerization of Snf7 is a crucial step in the formation of ESCRT-III, we hypothesize that either inhibiting Snf7 oligomerization or stabilizing Snf7 oligomers on endosomes could cause distinct sorting defects. To test this idea, we examined the fate of Mup1-GFP, a methionine transporter (Menant et al., 2006). Under steady-state conditions Mup1-GFP is almost exclusively localized to the plasma membrane (PM), and very little Mup1-GFP is present on intracellular membranes (Figure 6D). However, 1 hr after addition of methionine, Mup1-GFP was endocytosed from the PM and trafficked to the lumen of the vacuole (Figure 6D). Upon overexpression of Snf7, Mup1-GFP trafficked to the lumen of the vacuole and accumulated in large aberrant endosomal structures, reminiscent of class E compartments (maybe "mini-E") (Figure 6D, arrows), suggesting that MVB sorting had stalled. Similar results were obtained with GFP-CPS (Figure S4B). Importantly, overexpression of Snf7 does not bypass loss of the nucleator, Vps20 (Figure S4B). However upon loss of Snf7, Mup1-GFP accumulated on the E-compartment (arrowhead) as expected and was also detected at the plasma membrane (PM, arrow) (Figure 7A). Importantly, all ESCRT mutants that interfere with Snf7 oligomerization (e.g., *vps20Δ*) phenocopy the Mup1-GFP distribution in *snf7Δ* mutant (Figure 7B). In contrast, mutants that fail to terminate Snf7 oligomerization (*vps24Δ*, *vps2Δ*, and *vps4Δ*) and therefore fail to dissociate ESCRT-III had a different Mup1-sorting defect. Mup1-GFP accumulated almost exclusively on the E compartment (arrowhead), and very little Mup1-GFP was detected at the PM (Figures 7A and 7B). Loss of *DID2* had very little effect on Mup1-GFP sorting; however, overexpression of Snf7 resulted in a strong defect, similar to *vps24Δ* mutants. (Figure S4C).

Quantification of the fluorescence intensity (I_F) on the E compartment and at the PM allowed the calculation of a fluorescence ratio (F_R) (I_F at the E compartment divided by I_F at the PM) as a measure of Mup1-GFP subcellular distribution. A high F_R represents predominant localization of Mup1-GFP to the E compartment. Interestingly, ESCRT mutants clearly fall into two classes with respect to Mup1-GFP subcellular distribution. Class I mutants exhibited low F_R, meaning localization of Mup1-GFP at the PM and on the class E compartment. Class I included all ESCRT mutants in which Snf7 oligomerization fails (*vps36Δ*, *vps22Δ*, *vps20Δ*, *snf7Δ*, *snf7Δ/vps24Δ*) as well as ESCRT mutants that function early in the MVB pathway (*vps27Δ*, *vps23Δ*) (Figure 7B). Class II mutants had a high F_R and appeared to trap Mup1-GFP on the E compartment. It contained all ECSRT mutants that fail to terminate Snf7 oligomerization: *vps24Δ*, *vps2Δ*, and *vps4Δ* (Figure 7B). Thus we conclude that the formation of Snf7 oligomers is required to trap cargo at the E compartment.

To test if the difference in cargo distribution was due to cargo recycling from the E compartment back to the PM, we blocked vesicle fusion with the PM after methionine-induced internalization by using the temperature-sensitive *sec1-1* allele. Sixty minutes after methionine-induced internalization, cells were shifted to a nonpermissive temperature for another 60 min. In *sec1-1* cells, Mup1-GFP was localized to the lumen of the vacuole (Figure 7C). In *vps24Δ*, *sec1-1* mutants, Mup1-GFP exclusively localized to the E compartment (arrowhead). However, in *snf7Δ*, *sec1-1* mutants, Mup1-GFP accumulated on the E compartment (arrowhead) and in vesicular structures (arrow) close to the PM (Figure 7C).

These findings indicate that loss of Snf7 or failure to induce oligomerization permits cargo transport out of the E compartment and recycling to the PM. In contrast, stabilization of Snf7 oligomers traps cargo on endosomes. If correct, mutations that release Snf7 autoinhibition should trap cargo on endosomes, because release of autoinhibition should favor Snf7 polymerization over dissociation. In contrast, *snf7* mutants that do not localize to endosomes should permit cargo recycling. We therefore replaced the autoinhibitory region of Snf7 (aa 190–240) with a 3×Flag tag, thereby generating the C-terminally truncated *snf7^{190}Flag* mutant. This mutant, *snf7^{190}Flag*, was released from autoinhibition. *snf7^{190}Flag* localized to endosomes in a Vps20-dependent manner (Figure S5A) and readily oligomerized on endosomes as demonstrated by glycerol gradient centrifugation (Figure S5B). In the *snf7^{190}Flag* mutant, Mup1-GFP was trapped on endosomes (Figure 7D). In contrast, in the *snf7^{110}Flag* truncation mutant that fails to localize to endosomes (Figure S5A), Mup1-GFP was not trapped on endosomes (Figure 7D).

These findings strongly suggest that Snf7 oligomerization is required to trap cargo at the endosome. Snf7 oligomerization blocks cargo recycling, possibly by sequestering cargo in a MVB sorting domain and thereby committing cargo to complete the last step of MVB sorting.

DISCUSSION

The ESCRT machinery is essential for the sorting of ubiquitinated transmembrane proteins through the MVB pathway. The molecular architecture and stoichiometry of ESCRT-I and ESCRT-II have been characterized. Both ESCRT-I and -II are recruited as heteromeric complexes from the cytoplasm to endosomes, where they bind directly to ubiquitinated transmembrane cargo. They are critical in collecting and concentrating cargo proteins destined for sorting into MVBs.

Architecture and Stoichiometry of ESCRT-III In Vivo

Yeast genetics and biochemical experiments identified the core components of ESCRT-III: Vps20, Snf7, Vps24, and Vps2. The Vps20-Snf7 subcomplex was found to be required for the recruitment of the Vps2-Vps24 subcomplex (Babst et al., 2002a). The individual subunits are biochemically and structurally related. Each subunit contains 221–241 amino acids, an N-terminal basic and a C-terminal acidic region, and a core of an asymmetric antiparallel four-helix bundle (Muziol et al., 2006). To get a better understanding of the molecular mechanism of ESCRT-III assembly in the MVB sorting pathway, we characterized the architecture and stoichiometry of ESCRT-III in vivo. To this end, our results demonstrate that assembly of ESCRT-III on endosomes is a sequential process. It results in the formation of a transient 17.6S (450 kDa) complex that consists mainly of ESCRT-III subunits. ESCRT-I and ESCRT-II are no longer associated with ESCRT-III. Previous experiments indicated that only a small fraction of ESCRT-II interacts with ESCRT-III (Babst et al., 2002b). This interaction might be easily disrupted. Thus, the interactions of the different ESCRT complexes on endosomes appear to be dynamic. Vps20 functions as a nucleator, required to induce Snf7 oligomerization on endosomes. Vps24 terminates oligomerization, possibly by capping the Snf7 filament. Vps2 binds to Vps24 and subsequently recruits Vps4 to initiate dissociation of ESCRT-III. Consistent with this model, quantification experiments in vivo demonstrate that Snf7 is the most abundant ESCRT-III subunit. Given the high degree of conservation, ESCRT-III assembly in higher eukaryotes should follow similar rules (Vps20→Snf7→Vps24→Vps2). However, the situation might be more complex, since certain ESCRT-III subunits exist in multiple isoforms in mammals (e.g., ChMP4A, B, C).

We detect only Snf7 oligomers/filaments at endosomes in vivo, and we did not detect oligomerization of other ESCRT-III subunits. While that does not exclude the oligomerization of other ESCRT-III subunits in vivo, it suggests that the Snf7 oligomer is the major component of ESCRT-III and may drive late events in the MVB sorting reaction. Taking our quantitative data into consideration, we speculate that Vps20 could nucleate the polymerization of 10–15 Snf7 molecules before Vps24-dependent capping terminates the Snf7 filament. Interestingly, yeast two-hybrid studies showed that Snf7 or hSnf7 (Chmp4A, B, C) can interact with itself (Bowers et al., 2004; Martin-Serrano et al., 2003). Overexpression of Snf7, hSnf7, or hVps24, in which the autoinhibitory region was mutated, induced accumulation of ESCRT-III on endosomes or the PM (Lin et al., 2005; Zamborlini et al., 2006). Moreover, overexpressed hSnf7 can form extensive circular arrays of homopolymeric filaments in COS-7 cells. These ring-like hSnf7 filaments have the capacity to form spiraling filaments that tubulate away from the PM when an ATPase-defective Vps4 mutant was coexpressed (Hanson et al., 2008). Thus it appears that at high concentrations ESCRT-III subunits polymerize into long filaments.

Although we are just beginning to understand the molecular architecture of ESCRT-III, there are striking mechanistic analogies to filaments like actin or tubulin. ESCRT-III could form a polarized filament that has a nucleation and a capping site. Similar to actin-related proteins 2 and 3 (Arp2/3), Vps20, possibly in association with ESCRT-II, would nucleate polymerization of Snf7. Interestingly, Vps20 binds directly to the ESCRT-II subunit Vps25 (Teo et al., 2004). ESCRT-II contains two copies of Vps25 (Hierro et al., 2004; Teo et al., 2004), which could bind to and activate two copies of Vps20. Maybe two Vps20 molecules are required to increase the local concentration of Snf7 on endosomes and thereby nucleate its oligomerization. Therefore it will be interesting to determine if one or two Vps25 subunits are required to allow Vps20-dependent Snf7 oligomerization.

Dissociation of ESCRT-III requires a modular interaction of the MIM domain in Vps2 with the MIT domain in the AAA-ATPase Vps4 (Obita et al., 2007; Stuchell-Brereton et al., 2007). Interestingly, destabilization and severing of microtubules requires a similar modular interaction of an AAA-ATPase, spastin, with the acidic C terminus of β-tubulin (Roll-Mecak and Vale, 2008). However, there are fundamental differences. Actin and tubulin are nucleotide-binding proteins that function as ATPases and GTPases, respectively. The structure of hVps24 excludes this function for ESCRT-III subunits. Actin and tubulin form very large and yet dynamic filaments, whereas ESCRT-III filaments appear to be small and transient. While actin and tubulin form filaments in the cytoplasm, ESCRT-III forms oligomers on membranes.

Yet, it is very tempting to speculate that ESCRT-III forms a polar filament that assembles in a sequential manner. Our findings imply that the mechanism for assembly of ESCRT-III encodes

the information for the size of the Snf7 filament and the timing of its disassembly, suggesting that ESCRT-III has a built-in "timer" which is crucial for its function in MVB sorting.

Function of ESCRT-III in the MVB Pathway

While it is clear that each core subunit of ESCRT-III is essential for the function of the MVB pathway, the molecular details of ESCRT-III function in MVB sorting are not understood. Epitasis experiments indicate that ESCRT-III functions downstream of Vps27, ESCRT-I, and ESCRT-II (Babst et al., 2002b) and thus executes a late step in cargo sorting and MVB formation. Unlike Vps27, ESCRT-I, and ESCRT-II, ESCRT-III does not bind directly to ubiquitinated transmembrane proteins. Indeed ESCRT-III recruits via Bro1 the deubiquitinating enzyme Doa4 (Luhtala and Odorizzi, 2004), which removes ubiquitin prior to sorting cargo into MVB vesicles. How can cargo molecules, once deubiquitinated, complete MVB sorting? We found that oligomerization of Snf7 is a key event that is essential to trap cargo on endosomes. Interestingly, in HeLa cells, siRNA depletion of Hrs and ESCRT-I causes EGFR recycling and sustained signaling, whereas depletion of hVps24 results in EGFR accumulation on endosomes (Raiborg et al., 2007). These findings are largely consistent with our findings. Thus, we propose that Snf7 oligomerization defines a commitment point for cargo and controls the spatial distribution of cargo molecules on endosomes. Snf7 oligomers could do this in two different ways.

1. ESCRT-III could delay exit of cargo from endosomes by blocking access to sites for cargo recycling. How ESCRT-III would be positioned to act at these sites is not clear.
2. Snf7 filaments associated with endosomal membrane could delineate an MVB sorting domain and restrict lateral movement of cargo molecules, thereby keeping cargo committed to MVB sorting. Snf7 oligomerization requires ESCRT-II, which interacts directly with Vps20 and with ubiquitinated cargo. In close proximity to cargo, Snf7 oligomers could form rings, similar to the ring-like filaments generated by overexpression of hSnf7 (Hanson et al., 2008), to encircle cargo.

Clearly, this model does not yet provide the mechanism for membrane invagination and vesicle fission. Additional in vivo and in vitro experiments will be needed to address these important questions.

EXPERIMENTAL PROCEDURES

Materials

Goat polyclonal antibody specific for Vps36 was purchased from Santa Cruz. Mouse monoclonal specific for Pep12 was purchased form Invitrogen, and mouse monoclonal antibodies specific for Flag and Flag-agarose were purchased from Sigma. Rabbit polyclonal antibodies specific for Vps23 and Snf7 were described previously (Babst et al., 1998, 2000). DSP was from Pierce and FM4-64 from Invitrogen.

Strains and Media and DNA Manipulation

S. cerevisiae strains used in this work, media, and DNA manipulations are described in the Supplemental Data.

Velocity Sedimentation on 10%–40% Glycerol Gradients

Thirty OD_{600} equivalents of the yeast cells were spheroplasted and osmotically lysed in PBS (8 g/l NaCl, 0.2 g/l KCl, 1.44 g/l Na_2HPO_4, 0.24 g/l KH_2PO_4 [pH = 7.2]) containing protease inhibitors (Complete, Roche Molecular Biochemicals; Pepstatin A, Sigma) and subjected to subcellular fractionation as previously described (Babst et al., 1997). Membrane fractions (P13) and cytoplasm (S100) were solubilized in PBS, 0.2% Tween20. Linear glycerol gradients (10%–40%) + 0.2% Tween20 were prepared, and solubilized protein samples (equivalents of 30 OD_{600}) were loaded and sedimented for 210 min at 100,000 × g. One milliliter fractions were collected from the top of the gradient and TCA precipitated. Calibration of the gradient was performed using Aldolase, Catalase, Ferritin, and Thyroglobulin.

In Vivo Crosslinking

Thirty OD_{600} equivalents of the yeast cells were spheroplasted, washed in crosslinking buffer (20 mM HEPES, 0.7 M Sorbitol, 100 mM KCH_3COOH [pH = 7.4]), resuspended in 1 ml crosslinking buffer, and incubated with 5 μM DSP for 15 min. DSP was quenched with 100 mM TRIS (pH = 7.4).

Gel Filtration

Gel filtration was performed as previously described (Babst et al., 2000).

Coimmunoprecipitation

Thirty OD_{600} equivalents of the yeast cells were subjected to subcellular fractionation as previously described (Babst et al., 1997). Membrane fractions (P13) and cytoplasm (S100) were solubilized in PBS, 0.2% Tween20. Solubilized proteins were subjected to immunoprecipitation and incubated for 90 min with 15 μl α-Flag Agarose. α-Flag Agarose was washed four times with PBS, 0.2% Tween20 and one time with PBS. Bound proteins were eluted with SDS sample buffer.

Microscopy

For details please refer to Supplemental Data.

Image and FRET Analysis

Quantitative image analysis was used to determine the fluorescence intensity of GFP molecules. Pixel-by-pixel analysis was performed using Softworx Data-Inspector. The fluorescence intensity (I_F) of LacI-GFP was measured using a 5 × 5 pixel region of interest (ROI) and subtracted against the nuclear background (5 × 5 pixel ROI of LacI-GFP not present in the dot) (Figure S2A). Fluorescence images of all four ESCRT-III-GFP subunits were captured using identical microscope- and camera settings as well as excitation times (0.4 s) as for the LacI-GFP/LacO reporter system. I_F of ESCRT-III-GFP subunits was measured using 80 × 80 pixel ROI and subtracted against background (Figure S2A). Total cellular I_F was background-corrected and normalized to the I_F of 256 LacI-GFP molecules.

The I_F of Mup1-GFP was measured using a 19 × 19 pixel ROI on an E compartment (I_{FE}) or at the plasma membrane (I_{FPM}) and subtracted against background (19 × 19 pixel ROI outside cells). The ratio was calculated I_{FE} / I_{FPM}.

FRET-ratio calculations were performed as previously described (McIntyre et al., 2007; Muller et al., 2005). $FRET_R$ is measured as fluorescence intensities (I_F) in the mCherry channel after excitation of ESCRT-III-GFP. A considerable advantage $FRET_R$ is the independence from fluorophore concentration, but sensitivity is best for equimolar fluorophore concentrations. Therefore, $FRET_R$ is ideal to determine the formation of homo-oligomers that are both encoded from homologous genetic alleles and have very similar I_F (Figure S1D). ESCRT-III-GFP molecules were FRET donors and ESCRT-III-mCherry the FRET acceptors. For every analysis, 30 fields were captured in the following order, GFP, FRET, and mCherry, with 0.4 sec exposure and a least 49 cells analyzed. Image analysis was performed using Softworx (Applied Precision). Fluorescence intensities were measured using a 5 × 5 pixel ROI and subtracted against background (5 × 5 pixel ROI outside the cell). GFP and mCherry spillover factors were measured in ESCRT-III-GFP and ESCRT-III-mCherry cells. Spillover factors are measured as I_F in the donor channel without donor and I_F in the acceptor channel without the acceptor. The spillover factor (SF) is the intensity of the GFP signal in the FRET channel divided by its intensity in the GFP channel. Snf7-GFP was GSF = 0.067 ± 0.03 and for Snf7-mCherry CSF = 0.02 ± 0.01, for Vps20-GFP = 0.25 ± 0.12,

Vps24-GFP = 0.067 ± 0.015, Vps2-GFP = 0.082 ± 0.04, Vps24-mCherry = 0.047 ± 0.011, Vps2-mCherry = 0.056 ± 0.016. Total spillover in each measurement was determined using the following equation: $Spillover_{total}$ = (GSF × GFP) + (CSF × CFP). FRET ratio was calculated using: $FRET_R$ = FRET/$Spillover_{total}$ (Muller et al., 2005). No FRET results in $FRET_R$ = 1.

SUPPLEMENTAL DATA

Supplemental data include Supplemental Experimental Procedures, one table, and five figures and can be found with this article online at http://www.developmentalcell.com/cgi/content/full/15/4/578/DC1/.

ACKNOWLEDGMENTS

D.T. is funded by HFSP (LT00634/2006-L). S.S. is supported by a fellowship of the American Heart Association (AHA 0826060D). We are grateful to Xin Luo for excellent help in the quantification of Mup1-GFP localization and to Charles Lin for providing the Mup1-GFP construct. We would like to thank Roberto Botelho, Jason MacGurn, and Tony Bretscher for critically reading the manuscript.

Received: April 11, 2008
Revised: July 30, 2008
Accepted: August 22, 2008
Published: October 13, 2008

REFERENCES

Azmi, I.F., Davies, B.A., Xiao, J., Babst, M., Xu, Z., and Katzmann, D.J. (2008). ESCRT-III family members stimulate Vps4 ATPase activity directly or via Vta1. Dev. Cell *14*, 50–61.

Babst, M., Sato, T.K., Banta, L.M., and Emr, S.D. (1997). Endosomal transport function in yeast requires a novel AAA-type ATPase, Vps4p. EMBO J. *16*, 1820–1831.

Babst, M., Wendland, B., Estepa, E.J., and Emr, S.D. (1998). The Vps4p AAA ATPase regulates membrane association of a Vps protein complex required for normal endosome function. EMBO J. *17*, 2982–2993.

Babst, M., Odorizzi, G., Estepa, E.J., and Emr, S.D. (2000). Mammalian tumor susceptibility gene 101 (TSG101) and the yeast homologue, Vps23p, both function in late endosomal trafficking. Traffic *1*, 248–258.

Babst, M., Katzmann, D.J., Estepa-Sabal, E.J., Meerloo, T., and Emr, S.D. (2002a). Escrt-III: an endosome-associated heterooligomeric protein complex required for mvb sorting. Dev. Cell *3*, 271–282.

Babst, M., Katzmann, D.J., Snyder, W.B., Wendland, B., and Emr, S.D. (2002b). Endosome-associated complex, ESCRT-II, recruits transport machinery for protein sorting at the multivesicular body. Dev. Cell *3*, 283–289.

Bowers, K., Lottridge, J., Helliwell, S.B., Goldthwaite, L.M., Luzio, J.P., and Stevens, T.H. (2004). Protein-protein interactions of ESCRT complexes in the yeast Saccharomyces cerevisiae. Traffic *5*, 194–210.

Brickner, J.H., and Walter, P. (2004). Gene recruitment of the activated INO1 locus to the nuclear membrane. PLoS Biol. *2*, e342.

Dimaano, C., Jones, C.B., Hanono, A., Curtiss, M., and Babst, M. (2008). Ist1 regulates vps4 localization and assembly. Mol. Biol. Cell *19*, 465–474.

Hanson, P.I., Roth, R., Lin, Y., and Heuser, J.E. (2008). Plasma membrane deformation by circular arrays of ESCRT-III protein filaments. J. Cell Biol. *180*, 389–402.

Hierro, A., Sun, J., Rusnak, A.S., Kim, J., Prag, G., Emr, S.D., and Hurley, J.H. (2004). Structure of the ESCRT-II endosomal trafficking complex. Nature *431*, 221–225.

Hurley, J.H., and Emr, S.D. (2006). The ESCRT complexes: structure and mechanism of a membrane-trafficking network. Annu. Rev. Biophys. Biomol. Struct. *35*, 277–298.

Katzmann, D.J., Odorizzi, G., and Emr, S.D. (2002). Receptor downregulation and multivesicular-body sorting. Nat. Rev. Mol. Cell Biol. *3*, 893–905.

Lin, Y., Kimpler, L.A., Naismith, T.V., Lauer, J.M., and Hanson, P.I. (2005). Interaction of the mammalian endosomal sorting complex required for transport (ESCRT) III protein hSnf7-1 with itself, membranes, and the AAA+ ATPase SKD1. J. Biol. Chem. *280*, 12799–12809.

Luhtala, N., and Odorizzi, G. (2004). Bro1 coordinates deubiquitination in the multivesicular body pathway by recruiting Doa4 to endosomes. J. Cell Biol. *166*, 717–729.

Martin-Serrano, J., Yarovoy, A., Perez-Caballero, D., and Bieniasz, P.D. (2003). Divergent retroviral late-budding domains recruit vacuolar protein sorting factors by using alternative adaptor proteins. Proc. Natl. Acad. Sci. USA *100*, 12414–12419.

McIntyre, J., Muller, E.G., Weitzer, S., Snydsman, B.E., Davis, T.N., and Uhlmann, F. (2007). In vivo analysis of cohesin architecture using FRET in the budding yeast Saccharomyces cerevisiae. EMBO J. *26*, 3783–3793.

Menant, A., Barbey, R., and Thomas, D. (2006). Substrate-mediated remodeling of methionine transport by multiple ubiquitin-dependent mechanisms in yeast cells. EMBO J. *25*, 4436–4447.

Muller, E.G., Snydsman, B.E., Novik, I., Hailey, D.W., Gestaut, D.R., Niemann, C.A., O'Toole, E.T., Giddings, T.H., Jr., Sundin, B.A., and Davis, T.N. (2005). The organization of the core proteins of the yeast spindle pole body. Mol. Biol. Cell *16*, 3341–3352.

Muziol, T., Pineda-Molina, E., Ravelli, R.B., Zamborlini, A., Usami, Y., Gottlinger, H., and Weissenhorn, W. (2006). Structural basis for budding by the ESCRT-III factor CHMP3. Dev. Cell *10*, 821–830.

Nickerson, D.P., West, M., and Odorizzi, G. (2006). Did2 coordinates Vps4-mediated dissociation of ESCRT-III from endosomes. J. Cell Biol. *175*, 715–720.

Obita, T., Saksena, S., Ghazi-Tabatabai, S., Gill, D.J., Perisic, O., Emr, S.D., and Williams, R.L. (2007). Structural basis for selective recognition of ESCRT-III by the AAA ATPase Vps4. Nature *449*, 735–739.

Odorizzi, G., Katzmann, D.J., Babst, M., Audhya, A., and Emr, S.D. (2003). Bro1 is an endosome-associated protein that functions in the MVB pathway in Saccharomyces cerevisiae. J. Cell Sci. *116*, 1893–1903.

Piper, R.C., and Katzmann, D.J. (2007). Biogenesis and function of multivesicular bodies. Annu. Rev. Cell Dev. Biol. *23*, 519–547.

Raiborg, C., Malerod, L., Pedersen, N.M., and Stenmark, H. (2007). Differential functions of Hrs and ESCRT proteins in endocytic membrane trafficking. Exp. Cell Res. *314*, 801–813.

Roll-Mecak, A., and Vale, R.D. (2008). Structural basis of microtubule severing by the hereditary spastic paraplegia protein spastin. Nature *451*, 363–367.

Rue, S.M., Mattei, S., Saksena, S., and Emr, S.D. (2008). Novel ist1-did2 complex functions at a late step in multivesicular body sorting. Mol. Biol. Cell *19*, 475–484.

Saksena, S., Sun, J., Chu, T., and Emr, S.D. (2007). ESCRTing proteins in the endocytic pathway. Trends Biochem. Sci. *32*, 561–573.

Scott, A., Chung, H.Y., Gonciarz-Swiatek, M., Hill, G.C., Whitby, F.G., Gaspar, J., Holton, J.M., Viswanathan, R., Ghaffarian, S., Hill, C.P., and Sundquist, W.I. (2005a). Structural and mechanistic studies of VPS4 proteins. EMBO J. *24*, 3658–3669.

Scott, A., Gaspar, J., Stuchell-Brereton, M.D., Alam, S.L., Skalicky, J.J., and Sundquist, W.I. (2005b). Structure and ESCRT-III protein interactions of the MIT domain of human VPS4A. Proc. Natl. Acad. Sci. USA *102*, 13813–13818.

Shim, S., Kimpler, L.A., and Hanson, P.I. (2007). Structure/function analysis of four core ESCRT-III proteins reveals common regulatory role for extreme C-terminal domain. Traffic *8*, 1068–1079.

Slagsvold, T., Pattni, K., Malerod, L., and Stenmark, H. (2006). Endosomal and non-endosomal functions of ESCRT proteins. Trends Cell Biol. *16*, 317–326.

Strack, B., Calistri, A., Craig, S., Popova, E., and Gottlinger, H.G. (2003). AIP1/ALIX is a binding partner for HIV-1 p6 and EIAV p9 functioning in virus budding. Cell *114*, 689–699.

Stuchell-Brereton, M.D., Skalicky, J.J., Kieffer, C., Karren, M.A., Ghaffarian, S., and Sundquist, W.I. (2007). ESCRT-III recognition by VPS4 ATPases. Nature *449*, 740–744.

Teo, H., Perisic, O., Gonzalez, B., and Williams, R.L. (2004). ESCRT-II, an endosome-associated complex required for protein sorting: crystal structure and interactions with ESCRT-III and membranes. Dev. Cell *7*, 559–569.

von Schwedler, U.K., Stuchell, M., Muller, B., Ward, D.M., Chung, H.Y., Morita, E., Wang, H.E., Davis, T., He, G.P., Cimbora, D.M., et al. (2003). The protein network of HIV budding. Cell *114*, 701–713.

Williams, R.L., and Urbe, S. (2007). The emerging shape of the ESCRT machinery. Nat. Rev. Mol. Cell Biol. *8*, 355–368.

Zamborlini, A., Usami, Y., Radoshitzky, S.R., Popova, E., Palu, G., and Gottlinger, H. (2006). Release of autoinhibition converts ESCRT-III components into potent inhibitors of HIV-1 budding. Proc. Natl. Acad. Sci. USA *103*, 19140–19145.